Gondwana Research 18 (2010) 583–595

Contents lists available at ScienceDirect

Gondwana Research

journal homepage: www.elsevier.com/locate/gr

Age constraints on the formation and emplacement of Neoproterozoic ophiolites along the Allaqi–Heiani Suture, South Eastern Desert of Egypt

K.A. Ali [a,d,*], M.K. Azer [b], H.A. Gahlan [c], S.A. Wilde [d], M.D. Samuel [b], R.J. Stern [a]

[a] Geosciences Department, University of Texas at Dallas, 800 W Campbell Rd., Richardson, TX 75080, USA
[b] Geology Department, National Research Centre, Dokki-Cairo, Egypt
[c] Geology Department, Faculty of Science, Assiut University, Assiut 71516, Egypt
[d] Department of Applied Geology, Curtin University of Technology, Perth, 6845 WA, Australia

ARTICLE INFO

Article history:
Received 31 December 2009
Received in revised form 8 March 2010
Accepted 11 March 2010
Available online 17 March 2010

Keywords:
Neoproterozoic
Ophiolite
Arabian–Nubian Shield
U–Pb zircon age

ABSTRACT

Ophiolites are key components of the Neoproterozoic Arabian–Nubian Shield (ANS). Understanding when they formed and were emplaced is crucial for understanding the evolution of the ANS because their ages tell when seafloor spreading and terrane accretion occurred. The Yanbu–Onib–Sol Hamed–Gerf–Allaqi–Heiani (YOSHGAH) suture and ophiolite belt can be traced ~600 km across the Nubian and Arabian shields. We report five new SHRIMP U–Pb zircon ages from igneous rocks along the Allaqi segment of the YOSHGAH suture in southernmost Egypt and use these data in conjunction with other age constraints to evaluate YOSHGAH suture evolution. Ophiolitic layered gabbro gave a concordia age of 730 ± 6 Ma, and a metadacite from overlying arc-type metavolcanic rocks yielded a weighted mean $^{206}Pb/^{238}U$ age of 733 ± 7 Ma, indicating ophiolite formation at ~730 Ma. Ophiolite emplacement is also constrained by intrusive bodies: a gabbro yielded a concordia age of 697 ± 5 Ma, and a quartz-diorite yielded a concordia age of 709 ± 4 Ma. Cessation of deformation is constrained by syn- to post-tectonic granite with a concordia age of 629 ± 5 Ma. These new data, combined with published zircon ages for ophiolites and stitching plutons from the YOSHGAH suture zone, suggest a 2-stage evolution for the YOSHGAH ophiolite belt (~810–780 Ma and ~730–750 Ma) and indicate that accretion between the Gabgaba–Gebeit–Hijaz terranes to the south and the SE Desert–Midyan terranes to the north occurred as early as 730 Ma and no later than 709 ± 4 Ma.

1. Introduction

The Neoproterozoic Era was an important time of crustal growth, especially in the Arabian–Nubian Shield (ANS; Stern, 2008). The ANS is a collage of well-preserved tectonostratigraphic terranes (Fig. 1) with well-defined suture zones marked by ophiolites (Stoeser and Camp, 1985; Johnson and Woldehaimanot, 2003; Stern et al., 2004). Juvenile arc terranes formed around the margins of the Mozambique Ocean and collided to form the ANS during mid-Neoproterozoic (Cryogenian) time. Arc accretion ended by late Neoproterozoic time (~630 Ma) when large fragments of East and West Gondwana collided, closing the Mozambique Ocean and forming the East African–Antarctic Orogen (Stern, 1994; Jacobs and Thomas, 2004). ANS sutures are thus subdivided into older arc–arc sutures separating ~700–870 Ma arc terranes and younger arc–continent sutures which formed at ~630 Ma (Stoeser and Camp, 1985; Pallister et al., 1988; Kröner et al., 1992; Abdelsalam et al., 2003, 2008; El-Bialy, 2010).

Consensus exists that most ANS ophiolites are of the supra-subduction zone (SSZ) type; that is, they formed by seafloor spreading above an active subduction zone. Beyond this, there are several tectonic scenarios suggested for the formation of ANS ophiolites: (i) remnants of back-arc basins (Bakor et al., 1976; Frisch and Al-Shanti, 1977; Kröner, 1985; Pallister et al., 1988); (ii) fragments of normal oceanic crust (Zimmer et al., 1995); or (iii) forearc seafloor spreading during subduction initiation (Stern et al., 2004; Azer and Stern, 2007; Abd El-Rahman et al. 2009a). Different ophiolites may have formed in different SSZ tectonic settings. Distribution of the Neoproterozoic ophiolites in the ANS (Fig. 1) show that Jabal Ess and Jabal al Wask ophiolites are the main occurrences within the Yanbu suture zone of NW Arabia (Dilek and Ahmed, 2003). The Jabal Ess ophiolite has a Penrose-type complete pseudostratigraphy (Dilek and Ahmed, 2003). Pallister et al. (1988) obtained a U–Pb conventional multigrain zircon age of 706 ± 11 Ma for an isotropic gabbro intruded into the Ess ophiolite. In the Bir Umq suture

* Corresponding author. Geosciences Department, University of Texas at Dallas, 800 W Campbell Rd., Richardson, TX 75080, USA. Tel.: +1 2011 971 1156; fax: +1 972 883 2537.
E-mail address: alik6588@yahoo.com (K.A. Ali).

1342-937X/$ – see front matter
doi:10.1016/j.gr.2010.03.002

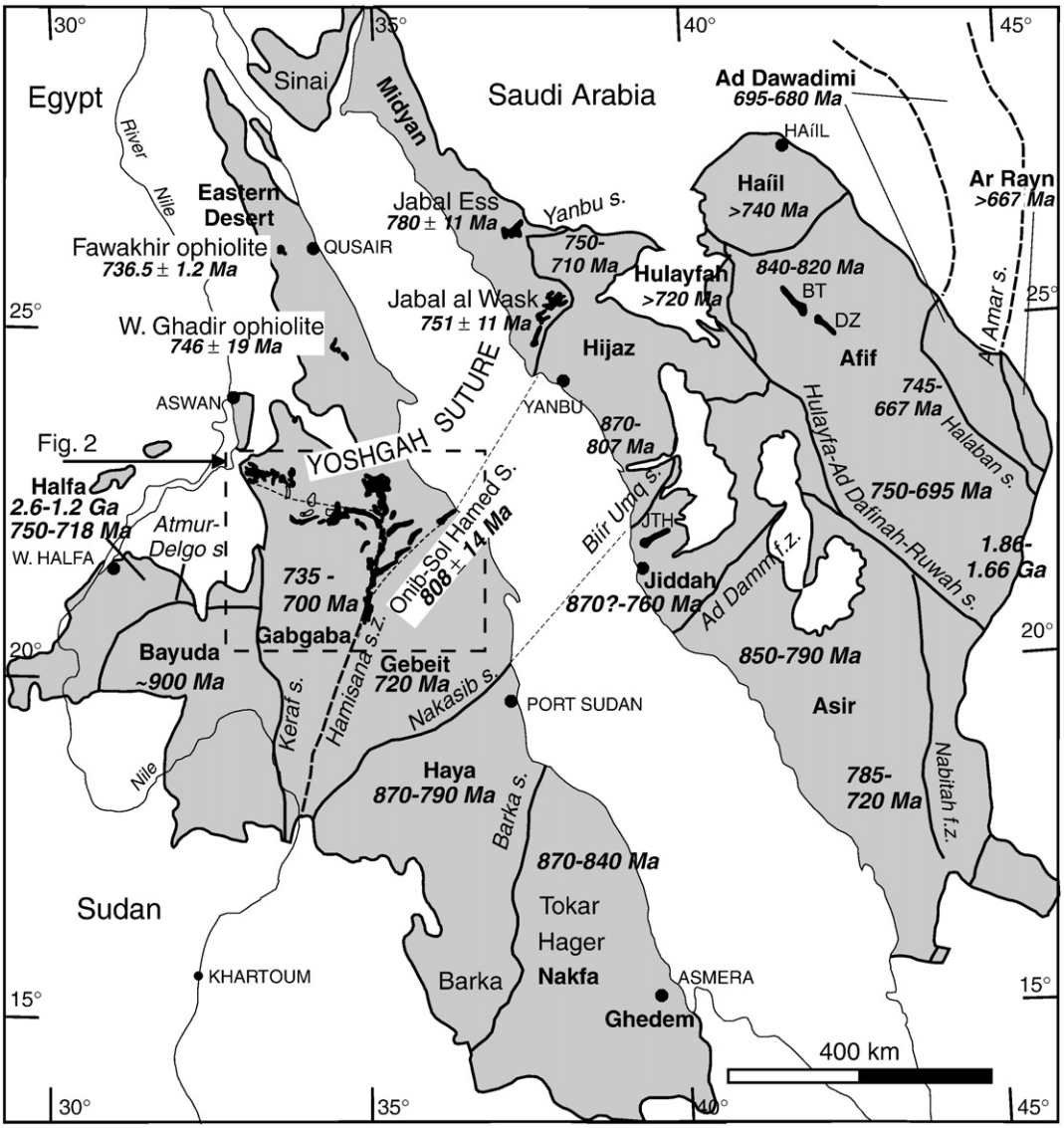

Fig. 1. Map of Arabian–Nubian Shield tectonostratigraphic terranes (modified from Johnson and Woldehaimanot, 2003), showing terrane ages from Stern et al. (1994), Stern et al. (1989), Kröner et al. (1992), Kröner et al. (1991), Pallister et al. (1988), Agar et al. (1992), Whitehouse et al. (2001), Hargrove et al. (2006a,b), Andresen et al. (2009), and Küster et al. (2008). Abbreviations for ophiolite names are: BT = Bir Tuluha; DZ = Darb Zubaydah; JTH = Jabal Thurwah. The location of Fig. 2 is indicated.

zone to the south, the Bir Umq and Jabal Thurwah ophiolites (Fig. 1) show characteristics of forerac and/or immature island-arc (Pallister et al., 1988; Dilek and Ahmed, 2003). The Jabal Thurwah ophiolite has a complete Penrose-type pseudostratigraphy (Dilek and Ahmed, 2003; Hargrove et al., 2006a). The Jabal Thurwah ophiolite was suggested to have formed in a supra-subduction zone based on the chemistry of the basaltic lavas (Nassief et al., 1984) whereas the ophiolites of Bir Tuluha and Darb Zabaydah in the Hulayfaf–Ruwah suture (Fig. 1) may have formed in a forearc (Dilek and Ahmed, 2003; Dilek et al., 2007). Pearce and Robinson (2010) suggested a two-stage model; following subduction initiation, mantle advects into the wedge and forms the ophiolite by sea-floor spreading, then subsequent influx of hot depleted mantle magma give another pulse of magma to produce the arc lavas. A coarse-grained gabbro from Jabal Thurwah ophiolite (Fig. 1) yielded a U–Pb zircon age of 777 ± 17 Ma with a few zircons that yielded an age of 1130 Ma, perhaps reflecting assimilation from older crust (Hargrove et al., 2006a). A plagiogranite dyke in serpentinized peridotites in the Bir Tuluha ophiolite (Fig. 1) yielded U–Pb zircon ages from 843 to 821 Ma (Pallister et al., 1988). The Wadi Ghadir ophiolite, Eastern Desert of Egypt (Fig. 1) is composed of layered and isotropic gabbro and pillow lavas intruded by dikes of different composition (Abd El-Rahman et al., 2009b). Based on the geochemical characteristics of the gabbro and pillow lavas in Wadi Ghadir area, it was suggested that the ophiolite formed in a back-arc basin above a NE-dipping subduction zone (Abd El-Rahman et al., 2009b). Kröner et al. (1992) obtained single zircon Pb–Pb evaporation age of 746 ± 19 Ma for a plagiogranite sample from Wadi Ghadir area (Fig. 1).

The Yanbu–Sol Hamed–Gerf–Allaqi–Heiani arc–arc suture is the northernmost ANS suture (Abdelsalam and Stern, 1996; Abdelsalam et al., 2003) and is the focus of this report. With the Red Sea closed, the suture extends ~E–W for at least 600 km, from the eastern edge of basement exposures in NW Arabia to the western edge of the shield in Egypt. Stern et al. (1990) named this the YOSHGAH suture (Fig. 1), an acronym that we adopt here. In this paper we help to resolve the age, evolution, and significance of ANS ophiolites by reporting single zircon SHRIMP ages for five igneous rocks along Wadi Allaqi, Egypt, the westernmost segment of the YOSHGAH suture. These data, when combined with published ages for other rocks of the YOSHGAH suture, are used to further constrain when the YOSHGAH ophiolites formed and terrane accretion along this suture occurred.

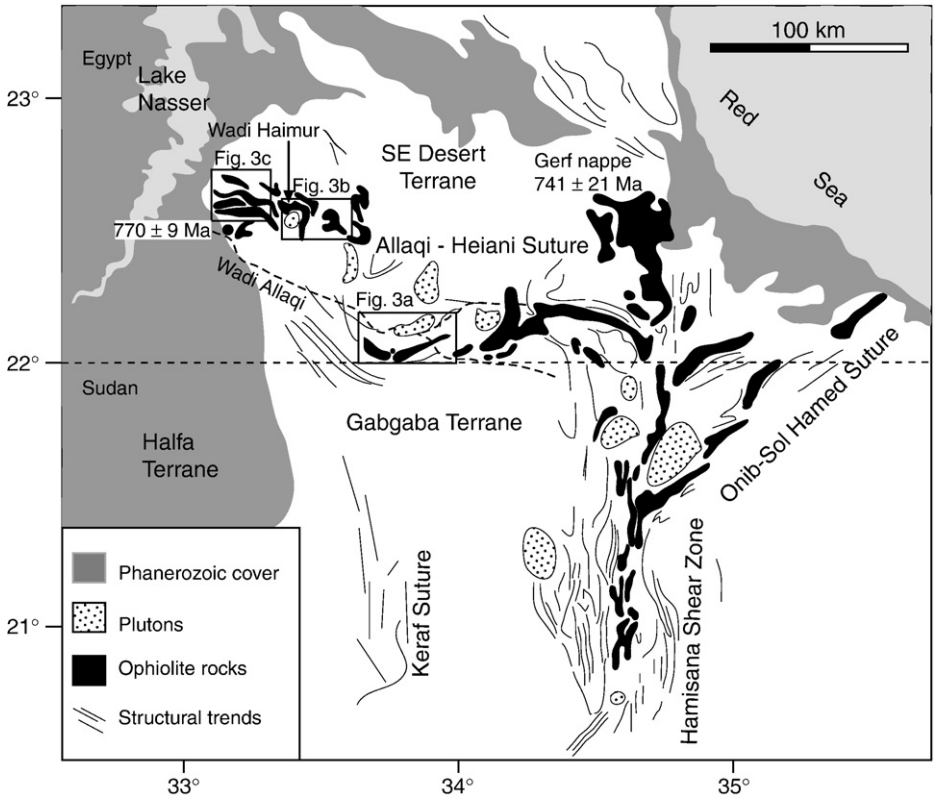

Fig. 2. Tectonic map of the Allaqi–Heiani–Gerf suture, South-Eastern Desert of Egypt (modified after Abdelsalam et al., 2003), showing location of ophiolites along the suture. Gerf ophiolite age from Kröner et al. (1992). The location of Fig. 3a, b and c is indicated.

2. Previous work

The YOSHGAH suture trends east from the entrance of Wadi Allaqi into Lake Nasser along the border between Egypt and Sudan to Jabal Gerf near the Red Sea (Fig. 2). Here, the suture is thought to be displaced southwards along the N–S Hamisana shear zone and continues NE along the Onib segment to the Red Sea, across which it can be traced into northwestern Saudi Arabia (Fig. 1). The Hamisana shear zone (Fig. 2) is an ophiolite-decorated post-accretionary structure (Stern et al., 1990) and not a suture as suggested by Berhe (1990). The YOSHGAH suture zone is broad and consists of four major lithologic associations: (i) ophiolites; (ii) island arc metavolcanic and metasedimentary successions; (iii) gabbroic to granitic intrusions; and (iv) gneiss (Stern et al., 1990; Kröner et al., 1992; Abd El-Naby and Frisch, 2002; Kusky and Ramadan, 2002; Abdelsalam et al., 2003; Zoheir and Klemm, 2007). The Allaqi segment of the YOSHGAH suture separates the SE segment of the Eastern Desert terrane in the north from the Gabgaba terrane in the south (Abdelsalam and Stern, 1996; Fig. 2). The ophiolite assemblages comprise one or more nappes composed mainly of mafic/ultramafic rocks and slices of serpentinite and talc-carbonate (Gahlan and Arai, 2009). Ophiolitic gabbroic rocks are mainly isotropic or layered metagabbros which are overlain by arc volcanic and volcaniclastic rocks and shelf metasediments. Stern et al. (1990) inferred that the Allaqi–Heiani ophiolitic nappe verged south during emplacement, and was then shortened E–W during terminal collision between E and W Gondwana at ~630 Ma. Arc metavolcanic rocks are metamorphosed to greenschist-facies (El-Nisr, 1997). Metasediments consist of marble, schist, greywacke and subordinate conglomerate (El Gaby et al., 1988; Gahlan and Arai, 2009).

An amphibolitic metamorphic sole at the base of the ophiolite is described at Wadi Haimur (Abd El-Naby et al., 2000). Metamorphism occurred during ophiolite emplacement, caused by thrusting of hot mantle peridotite on top of cold sediments and lavas (Abd El-Naby et al., 2000). Mineral assemblages in the sole record *P–T* conditions up to ~700 °C, 6.5–8.5 kbar in the south, but lower in the north (450–620 °C, 4.7–7.8 kbar).

Several efforts have been made to understand when YOSHGAH ophiolites formed and were obducted. We summarize these results from W to E. Zircons from a felsic dike intruding serpentinites near the extreme western end of the suture yielded Pb–Pb zircon evaporation ages of 3017 ± 3 Ma (AL-21) and 770 ± 9 Ma (AL17–20; Kröner et al., 1992). The Archean age was interpreted as due to zircon xenocrysts, whereas the younger date was taken as the age of the dike and thus a minimum age for ophiolite emplacement (Kröner et al., 1992) (Fig. 2).

Kröner et al. (1992) also obtained single zircon Pb–Pb evaporation ages of 729 ± 17 Ma and 736 ± 11 Ma for gabbro and diorite samples, respectively, from a single intrusion into sheared serpentinites in the Shilman area (Fig. 3b). They were not certain whether this gabbro-diorite body was part of the ophiolite or intruded it, but finally interpreted it as a post-obduction intrusion. In the Wadi Haimur area (due north of the Shilman area, Fig. 3b), Abd El-Naby et al. (2000) reported Sm/Nd dating of the ophiolite metamorphic sole. Whole-rock–metamorphic mineral pairs yielded similar ages of c. 630 Ma for clinopyroxene and hornblende, interpreted by Abd El-Naby et al. (2000) as a lower age limit for ophiolite formation and an upper age limit for metamorphism. They interpreted a ~590 Ma Sm/Nd age for a garnet-bearing metamorphic rock as approximating the timing of peak metamorphism. They also reported hornblende K/Ar ages of 570–550 Ma and interpreted these to reflect regional thermal events unrelated to ophiolite obduction. Independent evidence of ~600 Ma heating is given by a U–Pb zircon SHRIMP age of 603 ± 14 Ma for a post-tectonic granite in the Shilman area (Moussa et al., 2008; Fig. 3b), one of several within-plate granites in the region (El-Kazzaz and Taylor, 2001).

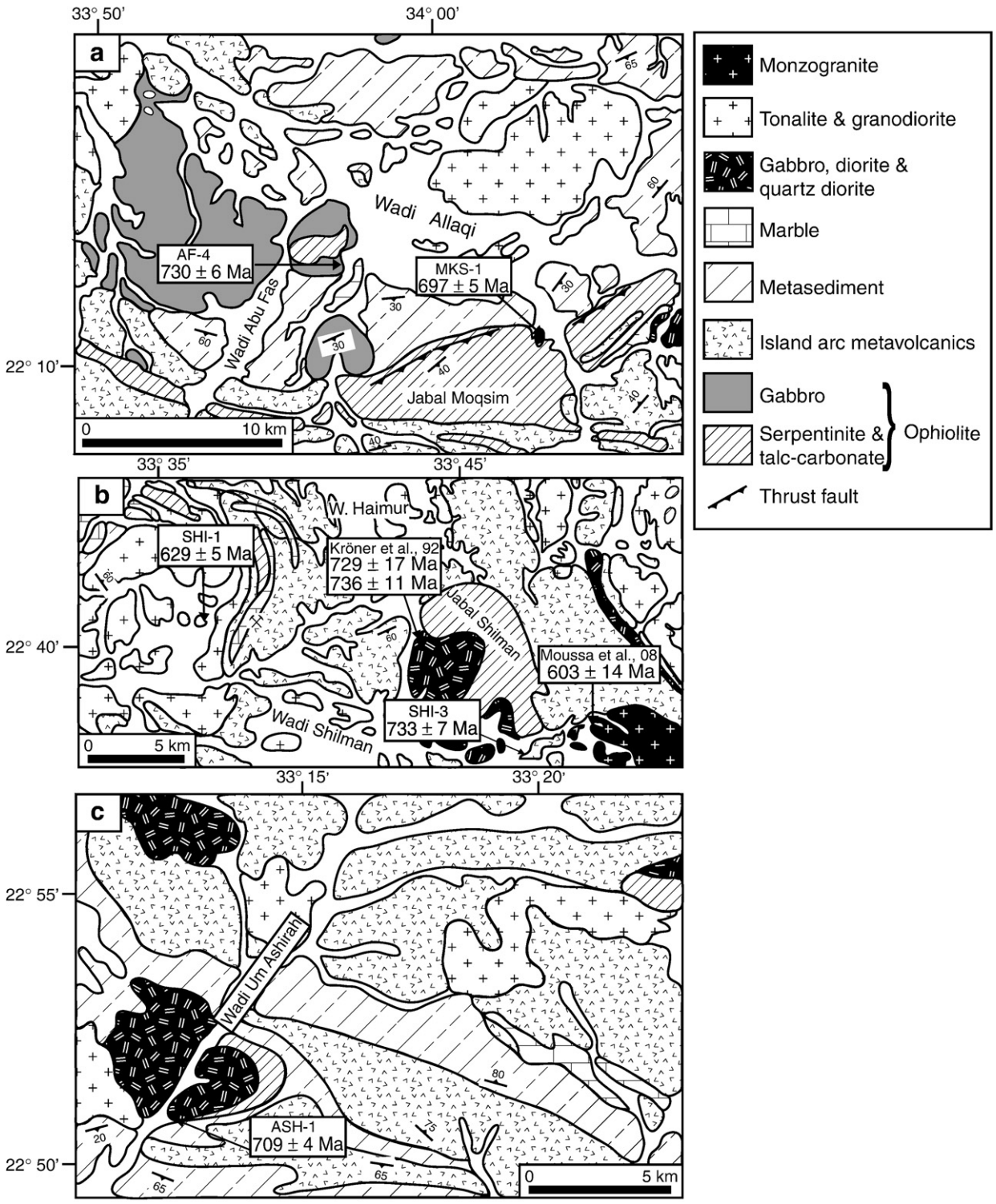

Fig. 3. Detailed geological maps of the study areas, showing the locations and ages of samples obtained during this and previous studies. Previous data sources: Kröner et al. (1992) and Moussa et al. (2008).

The Gerf ophiolite (Fig. 2) is unusually complete and has been dated by zircon Pb–Pb evaporation and Sm–Nd techniques. Kröner et al. (1992) reported a Pb–Pb single zircon evaporation age of 741 ± 21 Ma for a coarse-grained, layered gabbro. Zimmer et al. (1995) reported three Sm–Nd isochron ages: 1) whole rock gabbros (720 ± 9 Ma; $\varepsilon_{Nd} = +6.9 \pm 0.2$, MSWD = 11.5); 2) gabbro mineral separates 771 ± 58 Ma; $\varepsilon_{Nd} = +6.8 \pm 1.4$, MSWD = 1.4); and 3) ophiolitic metabasalts (758 ± 24 Ma; $\varepsilon_{Nd} = +7.6 \pm 0.9$, MSWD = 11.9). Based on these results, Zimmer et al. (1995) concluded that the Gerf ophiolite formed at ~750 Ma.

East of Gerf, the YOSHGAH suture is displaced to the south by the ~660–550 Ma N–S Hamisana Shear Zone (Fig. 2); the suture to the east is known as the Onib–Sol Hamed segment. A plagiogranite from the Onib ophiolite yielded a Pb–Pb evaporation age of 808 ± 14 Ma

(Kröner et al. 1992), significantly older than any other YOSHGAH ophiolite age.

The YOSGAH suture is traced into NW Arabia as the al Wask and Ess ophiolites. Jabal al Wask is among the largest ophiolites in the ANS (Fig. 1, Pallister et al., 1988). The ophiolite nappe is folded into a NE-trending synform above metavolcanic rocks and metasediments (Shanti and Roobol, 1979). The Jabal Ess ophiolite is a well-preserved allochthonous thrust sheet that, according to Pallister et al. (1988), contains all of the components of a classic ophiolite. They obtained a U–Pb conventional multigrain zircon age of 706 ± 11 Ma for trondhjemite intruded into the Ess ophiolite.

3. Analytical techniques

Five samples for age determination were collected during field studies in January 2009 from the Moqsim, Shilman, and Ashirah areas along Wadi Allaqi. Sample locations were determined using handheld GPS. Powders for chemical analysis were prepared at the University of Texas at Dallas (UTD) and analyzed for major and selected trace elements (Ba, Sr, Y, Sc, Zr, Be, and V) using fusion-ICP-MS whole rock techniques at ACTLABS, Canada (Table 1). Zircons were separated at UTD from five samples using crushing, heavy liquids and magnetic separation. Grains from the non-magnetic fractions were hand-picked, mounted on double-sided adhesive tape, and set in Epirez™ resin along with several grains of Sri Lanka zircon standard (CZ3) which has a conventionally measured $^{207}Pb/^{206}Pb$ age of 564 Ma (Pidgeon et al., 1994). The mounted zircons were ground and polished to effectively cut them in half and zircons were imaged by cathodoluminescence (CL) using a scanning electron microscope prior to gold coating. U–Th–Pb analyses were performed using the SHRIMP II ion microprobe at Curtin University following techniques described by Nelson (1997) and Williams (1998) utilizing five-cycle runs through the mass stations. A total of 58 spots on 54 zircons were analyzed, along with 17 analyses of the CZ3 standard, which yielded a 1σ variation in Pb/U isotopic ratios of 0.76% during the analytical session. Analytical results for zircons are listed in Table 2.

4. Sample locations, descriptions and geochronology results

We concentrated on three localities (Fig. 3) which we refer to (from E to W) as: Moqsim (Fig. 3a), Shilman (Fig. 3b), and Ashirah (Fig. 3c). The ophiolitic nappe in the Moqsim area comprises slices of serpentinites, talc-carbonates and metagabbros which are thrust over the arc metavolcanic–metasedimentary succession and intruded by granitic plutons (Fig. 3a). We sampled layered gabbro in Wadi Abu-Fas (Fig. 3a, sample AF-4) as well as gabbro near Jabal Moqsim (Fig. 3a, sample MKS-1). The ophiolite in the Shilman area (Fig. 3b) consists of sheared serpentinite; the ophiolite nappe is overlain by the arc metavolcanic–metasedimentary succession (Fig. 3b, sample SHI-3) and intruded by gabbro-diorite and syn to post-tectonic granitoids (Sample SHI-1). The syn-tectonic granitoids (Table 1; sample SHI-1) include granodiorite, interpreted as arc-related and I-type (El-Kazzaz and Taylor, 2001). The ophiolitic nappe in the Ashirah area comprises slices of serpentinite and talc-carbonate which are thrust over the arc metavolcanic–metasedimentary succession and intruded by gabbro-diorite plutons (Fig. 3c, Sample ASH-1).

Table 1
Major and selected trace elements for samples from Wadi Allaqi, Egypt.

Sample #	AF-4 gabbro	MKS-1 gabbro	SHI-3 dacite	SHI-1 granodiorite	ASH-1 qz-diorite
SiO_2 (%)	49.4	48.1	65.1	70.8	70.0
TiO_2	0.22	0.83	0.54	0.34	0.61
Al_2O_3	17.9	14.3	15.3	14.8	14.3
Fe_2O_3	5.36	9.28	5.61	2.77	4.73
MnO	0.09	0.13	0.10	0.05	0.05
MgO	10.03	11.49	1.74	0.72	0.90
CaO	10.75	9.19	2.86	2.63	3.77
Na_2O	2.48	2.79	4.45	3.96	4.20
K_2O	0.19	0.65	2.81	3.15	0.55
P_2O_5	0.02	0.14	0.14	0.12	0.11
Total	98.7	99.34	99.5	99.9	99.6
LOI	2.37	2.45	0.79	0.60	0.42
Ba (ppm)	52	62	690	517	238
Sr	445	468	177	214	393
Y	23	26	30	46	17
Sc	22	30	14	6	6
Zr	21	67	202	237	477
Be	<1	<1	1	7	1
V	97	180	84	24	38

Major (wt.%) and trace (ppm) elements analyzed by fusion-ICP.

4.1. Wadi Abu-Fas layered gabbro

Sample AF-4 (22.226°N, 33.951°E) is a sample from ~150 m thick lens of coarse-grained layered gabbro in the Moqsim area (Fig. 3a). This gabbro occurs within ophiolitic serpentinite, talc-carbonate, and dunite with spinel-rich bands. Thin-section examination (Fig. 4a) shows that the gabbro consists mainly of plagioclase, hornblende and pyroxene; plagioclase crystals are euhedral to subhedral, zoned and moderately altered. Plagioclase shows ophitic to subophitic texture with pyroxene. Clinopyroxene is altered to actinolite and chlorite; accessory minerals are Fe–Ti oxides, apatite and zircon. This sample contains 49.4% SiO_2 and has high MgO (10%) and low TiO_2 (0.22%) and K_2O (0.19%; Table 1), consistent with formation by crystal accumulation from a MORB-type melt. Zircons separated from sample AF-4 are euhedral to subhedral (100–200 μm) and yellow to pale brown in color. CL images show well-developed zoning as expected for magmatic zircons (Fig. 5a). One measurement was made on each of twelve grains (Table 2). Six spots show reverse discordance, have high common ^{206}Pb and were not used in the age calculation. The remaining six analyses are concordant and yield a weighted mean $^{206}Pb/^{238}U$ age of 730 ± 6 Ma (2σ; MSWD = 0.43; Fig. 6a). We interpret this as approximating the formation age of the Allaqi ophiolite in the Moqsim area.

4.2. Jabal Moqsim gabbro

Sample MKS-1 (22.186°N, 34.053°E) is a dark gray, coarse-grained gabbro collected from a small wadi east of Jabal Moqsim (Fig. 3a). Most of the ophiolite nappe consists of serpentinite and talc-carbonate. A small (~50 m diameter) body of gabbro appears to intrude the ophiolite nappe. Thin-section examination shows that the gabbro consists of altered plagioclase, clinopyroxene (altered to actinolite), and accessory apatite, Fe-oxides and zircon (Fig. 4b). The sample is mafic (SiO_2 = 48.1 wt.%; and has high MgO (11.5%) but with significantly higher concentrations of TiO_2 (0.83%) and K_2O (0.65%; Table 1) than the Abu-Fas ophiolitic gabbro to the west. Only four zircons were separated from this sample; these are euhedral, acicular, and yellowish brown in color (Fig. 5b). A total of 8 measurements were made on the four zircons (Table 2; Fig. 6b). The U content varies from 519 to 1505 ppm and Th/U is high (0.65–1.24), as expected for magmatic zircons. One spot (MKS-1.1a) has high common ^{206}Pb (Table 1) and a younger $^{207}Pb/^{206}Pb$ age (622 ± 44 Ma) than the other 7 analyses, perhaps due to a late thermal event, or related to intrusion of post-tectonic granites or dikes. Two analyses (MKS-1.2b and MKS-1.3a) show reverse concordance, have high U contents (1250 and 1505 ppm, respectively), and higher $^{206}Pb/^{238}U$ ages (720 and 731 Ma, respectively). These may be xenocrysts from the ophiolitic gabbro or the arc metavolcanic rocks in the area. The remaining five analyses are concordant and grouped tightly, defining a concordia age of 697 ± 5 Ma (95% conf.; MSWD = 0.091; Fig. 6b). We interpret this

Table 2
SHRIMP Th–U–Pb zircon data for samples from Wadi Allaqi, south Eastern Desert of Egypt.

Spot no.	U ppm	Th ppm	Th/U	Pb ppm	$^{204}Pb/^{206}Pb$	$^{208}Pb/^{232}Th$	% error	f206 %	$^{207}Pb^a/^{206}Pb^a$	% error	$^{206}Pb^a/^{238}U$	% error	$^{207}Pb^a/^{235}U$	% error	$^{208}Pb^a/^{232}Th$	% error	AGE 204 correction					
																	$^{208}Pb/^{232}Th$	1σ error	$^{207}Pb^a/^{206}Pb^a$	1σ error	$^{206}Pb^a/^{238}U$	1σ error
AF-4																						
AF-4.1[b]	43	10	0.23	4	0.00063	0.0395	4.64	1.13	0.0571	7.59	0.117	1.371	0.918	7.71	0.027	19.67	546	106	495	167	711	9
AF-4.2[b]	91	68	0.75	9	0.00092	0.0384	2.02	1.65	0.0563	6.71	0.119	1.129	0.927	6.80	0.033	4.86	654	31	462	149	728	8
AF-4.3[b]	144	150	1.04	14	0.00057	0.0367	1.59	1.02	0.0588	4.30	0.116	0.983	0.945	4.41	0.034	2.50	683	17	561	94	710	7
AF-4.4[b]	152	98	0.64	15	0.00058	0.0370	2.17	1.03	0.0580	4.19	0.117	0.979	0.934	4.31	0.033	3.79	661	25	531	92	712	7
AF-4.5[b]	223	95	0.43	22	0.00052	0.0385	1.83	0.92	0.0600	3.40	0.114	1.005	0.947	3.55	0.033	4.27	662	28	604	74	699	7
AF-4.6[b]	213	125	0.59	21	0.00046	0.0348	1.62	0.83	0.0599	3.07	0.115	0.914	0.948	3.20	0.031	3.10	625	19	598	66	701	6
AF-4.7	194	148	0.76	20	0.00050	0.0376	1.47	0.89	0.0630	3.12	0.120	0.929	1.046	3.25	0.035	2.55	689	17	708	66	733	6
AF-4.8	59	42	0.71	6	0.00075	0.0381	2.68	1.34	0.0588	7.63	0.118	1.510	0.959	7.78	0.033	5.98	665	39	559	166	721	10
AF-4.9	179	155	0.87	18	0.00033	0.0382	1.46	0.58	0.0661	3.43	0.120	0.940	1.091	3.56	0.037	2.51	726	18	810	72	729	6
AF-4.10	159	151	0.95	17	0.00033	0.0367	1.50	0.60	0.0611	2.79	0.121	0.946	1.019	2.95	0.035	2.04	699	14	644	60	736	7
AF-4.11	150	105	0.70	15	0.00032	0.0401	1.71	0.57	0.0674	4.96	0.120	1.012	1.113	5.06	0.038	4.03	755	30	849	103	729	7
AF-4.12	132	99	0.75	14	0.00037	0.0373	1.75	0.66	0.0632	2.52	0.119	0.974	1.040	2.70	0.035	2.30	699	16	715	53	727	7
MKS-1																						
MKS-1.1a[b]	556	362	0.65	52	0.00045	0.03461	1.18	0.80	0.0605	2.05	0.109	0.841	0.909	2.22	0.032	1.92	634	12	622	44	667	5
MKS-1.1b	1156	1077	0.93	114	0.00007	0.03466	0.95	0.13	0.0630	0.56	0.115	0.815	0.999	0.99	0.034	0.97	682	6	709	12	702	5
MKS-1.2a	777	835	1.07	76	0.00003	0.03471	0.93	0.04	0.0631	0.54	0.113	0.790	0.986	0.96	0.035	0.93	688	6	710	12	692	5
MKS-1.2b[b]	1250	1273	1.02	127	0.00002	0.035	0.89	0.03	0.0627	0.52	0.118	0.784	1.021	0.94	0.035	0.91	694	6	698	11	720	5
MKS-1.3a[b]	1505	1868	1.24	155	0.00000	0.03616	0.86	0.01	0.0625	0.48	0.120	0.781	1.035	0.92	0.036	0.86	718	6	692	10	731	5
MKS-1.3b	535	360	0.67	52	0.00010	0.03494	1.20	0.17	0.0617	1.04	0.113	0.814	0.965	1.32	0.034	1.26	682	8	664	22	693	5
MKS-1.4a	519	567	1.09	51	0.00012	0.03564	1.07	0.22	0.0612	1.25	0.114	0.893	0.965	1.54	0.035	1.14	699	8	645	27	698	6
MKS-1.4b	654	806	1.23	64	0.00003	0.03406	0.97	0.05	0.0625	1.82	0.114	0.814	0.983	1.99	0.034	1.22	675	8	690	39	697	5
SHI-3																						
SHI-3.3[b]	168	114	0.67	17	0.00045	0.0359	1.749	0.79	0.0585	4.77	0.118	1.051	0.951	4.88	0.033	3.92	657	25	550	104	718	7
SHI-3.4	115	78	0.68	12	0.00042	0.03741	1.96	0.74	0.0613	4.20	0.123	1.044	1.035	4.32	0.035	3.70	688	25	649	90	745	7
SHI-3.2	131	98	0.75	14	0.00053	0.03788	1.803	0.94	0.0622	3.94	0.121	1.008	1.037	4.06	0.035	3.22	690	22	680	84	736	7
SHI-3.1[b]	202	216	1.07	20	0.00057	0.03641	2.714	1.02	0.0589	4.51	0.115	0.979	0.936	4.61	0.034	3.36	679	22	562	98	704	7
SHI-3.5	207	216	1.04	21	0.00009	0.03602	1.436	0.17	0.0640	2.24	0.118	0.914	1.038	2.42	0.036	1.74	708	12	742	47	717	6
SHI-3.6	237	176	0.74	24	0.00010	0.03712	1.435	0.17	0.0633	1.15	0.120	0.884	1.045	1.45	0.037	1.47	726	10	717	24	729	6

SHI-3.7	149	147	0.99	15	0.00031	0.03709	1.574	0.55	0.0626	2.98	0.120	0.968	1.032	3.13	0.036	2.11	710	15	696	63	728	7
SHI-3.8[b]	74	74	1.00	8	0.00085	0.03681	2.166	1.51	0.0557	12.30	0.119	1.383	0.918	12.37	0.033	6.46	657	42	441	274	728	10
SHI-3.9	206	197	0.96	22	0.00006	0.03562	1.434	0.11	0.0646	1.37	0.122	0.904	1.087	1.65	0.035	1.51	702	10	763	29	741	6
SHI-3.10[b]	91	64	0.70	9	0.00029	0.03636	2.18	0.52	0.0592	4.12	0.120	1.079	0.982	4.26	0.035	3.25	686	22	575	90	732	7
SHI-3.11	95	60	0.63	10	0.00034	0.03772	2.158	0.61	0.0623	3.73	0.120	1.066	1.028	3.88	0.035	3.53	702	24	686	80	728	7
SHI-3.12	172	175	1.02	18	0.00013	0.03547	1.531	0.23	0.0625	3.14	0.120	0.954	1.031	3.28	0.035	2.15	694	15	693	67	728	7
SHI-3.13	167	160	0.96	17	0.00014	0.03672	1.526	0.25	0.0637	4.69	0.122	0.993	1.072	4.79	0.036	2.98	716	21	733	99	742	7
SHI-3.14[b]	111	73	0.66	11	0.00064	0.0377	2.052	1.14	0.0574	3.37	0.119	1.017	0.946	3.52	0.033	3.03	664	20	508	74	728	7
SHI-3.15	101	64	0.63	11	−0.0001	0.03874	2.216	−0.12	0.0672	4.02	0.122	1.202	1.126	4.20	0.039	2.42	777	18	843	84	740	8
SHI-1																						
SHI-1.1[b]	2555	66	0.03	233	0.00003	0.03436	2.0	0.05	0.0606	0.42	0.106	0.773	0.887	0.88	0.030	5.09	598	30	627	9	650	5
SHI-1.2	448	245	0.54	39	0.00024	0.03207	1.3	0.42	0.0599	1.83	0.102	0.827	0.842	2.01	0.030	1.98	606	12	599	40	626	5
SHI-1.3[b]	832	212	0.25	44	0.00060	0.02754	1.7	1.06	0.0569	3.88	0.062	0.839	0.487	3.97	0.022	6.06	444	27	489	86	388	3
SHI-1.4[b]	700	94	0.13	55	0.00033	0.03617	1.6	0.58	0.0609	1.52	0.092	0.810	0.770	1.72	0.028	5.30	558	29	637	33	565	4
SHI-1.5	700	332	0.47	61	0.00022	0.0342	1.2	0.40	0.0606	2.00	0.102	0.814	0.850	2.16	0.032	2.23	646	14	625	43	625	5
SHI-1.9[b]	449	123	0.27	36	0.00027	0.02836	1.8	0.48	0.0606	1.97	0.094	0.842	0.782	2.14	0.025	4.01	499	20	625	43	577	5
SHI-1.11	2692	463	0.17	236	0.00001	0.03191	1.1	0.02	0.0610	0.37	0.102	0.787	0.859	0.87	0.032	1.13	630	7	639	8	627	5
SHI-1.12	677	42	0.06	60	0.00006	0.0294	2.5	0.11	0.0606	1.19	0.104	0.806	0.866	1.44	0.026	10.27	510	52	623	26	636	5
SHI-1.13	599	379	0.63	52	0.00018	0.0314	1.2	0.31	0.0593	1.37	0.101	0.815	0.828	1.59	0.030	1.47	605	9	576	30	622	5
SHI-1.14	2125	46	0.02	190	0.00005	0.0350	2.3	0.09	0.0605	0.51	0.104	0.777	0.867	0.93	0.026	9.48	513	48	620	11	638	5
SHI-1.15[b]	1920	331	0.17	175	0.00011	0.03509	1.1	0.20	0.0607	0.64	0.106	0.778	0.887	1.01	0.033	1.81	647	12	628	14	649	5
ASH-1																						
ASH-1.1	164	38	0.23	16	0.00021	0.0400	2.50	0.38	0.0631	1.55	0.116	1.139	1.014	1.93	0.036	3.15	717	22	713	33	710	8
ASH-1.2	927	237	0.26	94	0.00008	0.0358	1.27	0.14	0.0620	1.59	0.117	0.835	1.004	1.80	0.034	3.19	685	21	675	34	716	6
ASH-1.3	520	138	0.27	52	0.00005	0.0359	1.48	0.09	0.0629	1.01	0.117	0.820	1.012	1.30	0.035	2.06	698	14	703	21	712	6
ASH-1.4	205	59	0.29	20	0.00024	0.0375	2.08	0.43	0.0612	2.87	0.114	0.920	0.964	3.02	0.034	5.13	676	34	646	62	697	6
ASH-1.5	426	164	0.38	42	0.00003	0.0353	1.41	0.06	0.0629	2.97	0.116	0.859	1.006	3.10	0.035	4.17	693	28	706	63	707	6
ASH-1.6	244	64	0.26	25	0.00008	0.0373	1.98	0.13	0.0633	5.56	0.118	0.976	1.029	5.64	0.036	10.99	715	77	718	118	719	7
ASH-1.7	626	115	0.18	62	0.00013	0.0365	1.81	0.23	0.0631	1.32	0.115	1.137	1.001	1.74	0.033	3.85	665	25	713	28	702	8
ASH-1.8[b]	2722	662	0.24	291	0.00001	0.0367	0.94	0.02	0.0625	0.29	0.124	0.772	1.073	0.83	0.037	0.95	725	7	691	6	756	6
ASH-1.9	382	113	0.29	37	0.00015	0.0356	1.60	0.27	0.0633	1.10	0.114	0.840	0.998	1.38	0.033	2.07	665	14	717	23	698	6
ASH-1.10	295	127	0.43	29	0.00004	0.0350	1.59	0.08	0.0637	0.97	0.116	0.862	1.018	1.30	0.035	1.67	687	11	732	21	707	6
ASH-1.11	577	234	0.41	58	0.00017	0.0363	1.24	0.30	0.0624	1.18	0.117	0.817	1.003	1.44	0.035	1.77	687	12	687	25	711	6
ASH-1.12	520	228	0.44	52	0.00011	0.0378	1.25	0.20	0.0636	1.70	0.117	0.827	1.027	1.89	0.037	2.19	729	16	728	36	714	6

[a] Common lead corrected using the measured ^{204}Pb.
[b] Indicates data excluded from calculated age.

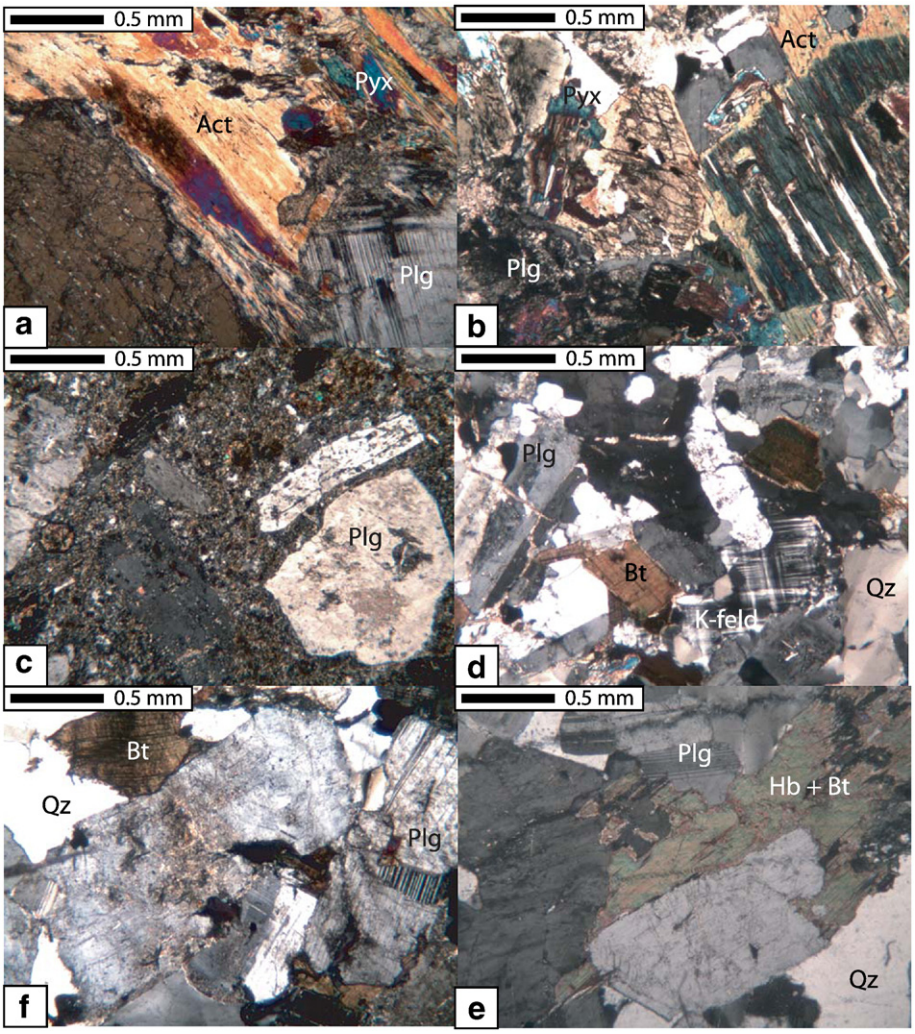

Fig. 4. Photomicrographs (cross-polarized light) of samples studied here. (a) Layered gabbro (sample AF-4) from Wadi Abu Fas; (b) Gabbro (sample MKS-1) from Jabal Moqsim; (c) Metadacite (sample SHI-3) from Wadi Shilman; (d) Granodiorite (sample SHI-1) from Wadi Shilman; (e) and (f) quartz diorite (sample ASH-1) from Wadi Um Ashirah. Qz = quartz, Plg = plagioclase, Bt = biotite, Hb = hornblende, Act = actinolite, Pyx = pyroxene, and K-feld = alkali feldspar. See text for details.

as the age of intrusion and crystallization of the gabbro into the already sheared serpentinite of the ophiolite.

4.3. Wadi Shilman metavolcanic rocks

Sample SHI-3 (22.631°N, 33.766°E) is a metadacite from the Shilman area where arc volcanic rocks overlie the ophiolite (Fig. 3b). The ophiolitic nappe is dominated by sheared serpentinite intruded by undeformed gabbro and diorite. SHI-3 consists of euhedral to subhedral phenocrysts of altered plagioclase in a fine-grained matrix of plagioclase, quartz and mafic minerals (Fig. 4c). Accessory minerals include Fe-oxides and zircon. Sample SHI-3 has high SiO_2 (65.1%) and K_2O (2.8%) but low MgO (1.74%) and TiO_2 (0.54%; Table 1). This metadacite is compositionally similar to arc metavolcanic rocks studied along Wadi Allaqi to the NW (El-Nisr, 1997) and may be part of the same metavolcanic succession. Zircons separated from sample SHI-3 are euhedral, stubby, pale-brown in color with well-developed magmatic oscillatory zoning (Fig. 5c). One analysis was made of each of 15 zircons (Table 2; Fig. 7a). These zircons contain moderate U contents (74–237 ppm) and have Th/U in the range expected for igneous zircons (0.63–1.07). Four analyses show reverse discordance (Fig. 7a) and have relatively high common ^{206}Pb; one spot (SHI-3.8) has the highest common ^{206}Pb (1.51, Table 2); these were not included in the age calculation. The remaining ten analyses yield a weighted mean $^{206}Pb/^{238}U$ age of 733 ± 7 Ma (95% conf.; MSWD = 1.8; Fig. 7a), which is taken as the crystallization age of the dacite. This age is indistinguishable from that of the underlying ophioliic gabbro sampled at Abu Fas (730 ± 6 Ma).

4.4. Wadi Shilman granodiorite

Sample SHI-1 (22.683°N, 33.597°E) is a granodiorite collected from the Shilman area (Fig. 3b). These syntectonic granitoids are interpreted as arc-related and I-type, based on their chemical signature (El-Kazzaz and Taylor, 2001). Sample SHI-1 is fine- to medium-grained, with hypidiomorphic granular texture (Fig. 4d). It consists mainly of zoned plagioclase with altered cores and less altered rims, perthitic K-feldspars, anhedral quartz and biotite with inclusions of accessory titanite, apatite and zircon, together with magnetite and ilmenite. The sample has high SiO_2 (70.8%) and K_2O (3.15%), and low MgO (0.72%) and TiO_2 (0.34%). Zircons are acicular and pale brown in color; CL images show well-developed oscillatory zoning, typical of magmatic zircons (Fig. 5d). One analysis was made for each of 11 zircons (Table 2) and results are presented on a concordia plot (Fig. 7b). Uranium contents are high (448–2692 ppm), and Th/U ratios are generally low (0.02 to 0.63). Two spots (SHI-1.1

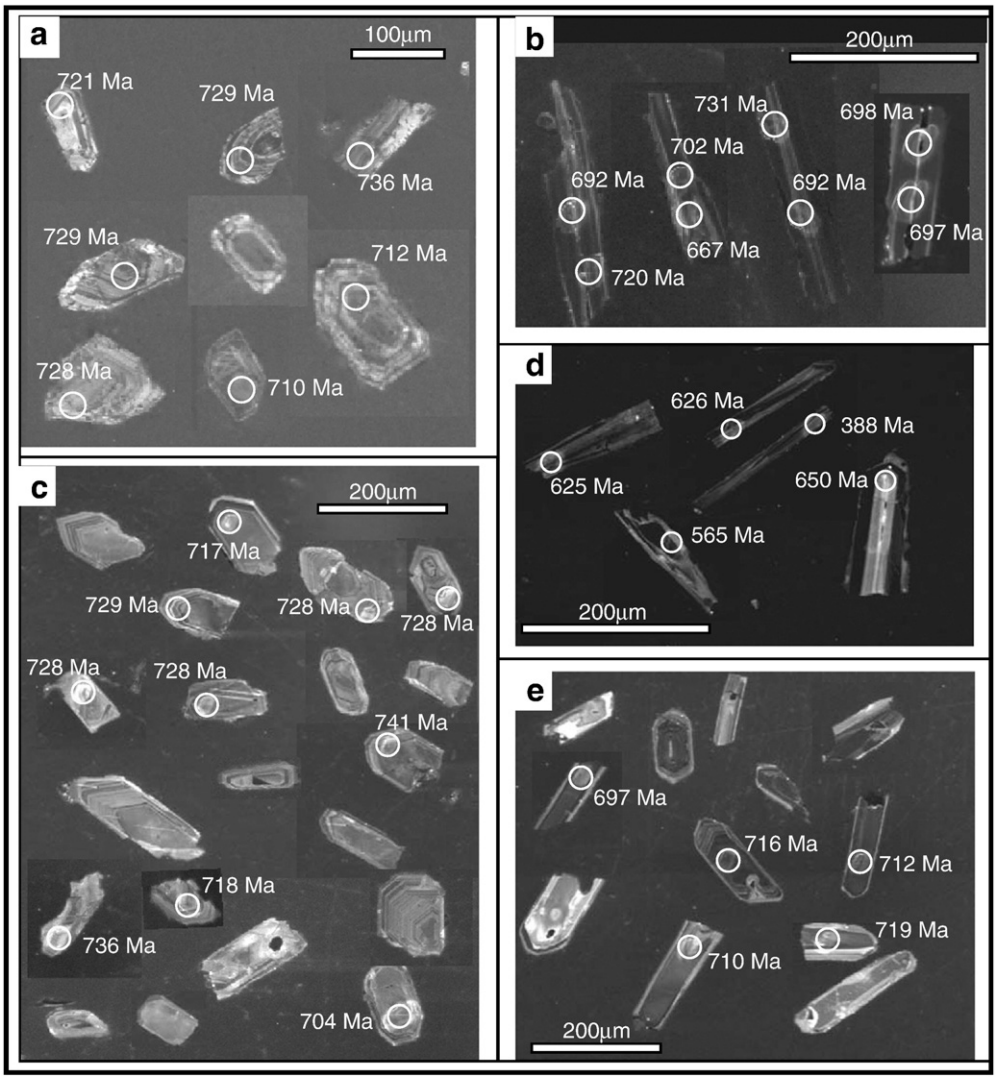

Fig. 5. Cathodoluminescence images of zircons from Wadi Allaqi samples; (a) Wadi Abu-Fas layered gabbro, (b) Jabal Moqsim gabbro, (c) Wadi Shilman metadacite, (d) Wadi Shilman granodiorite and (e) Wadi Um Ashirah quartz diorite.

and SHI-1.15) have high U contents (2555 and 1920 ppm, respectively) and record older $^{206}Pb/^{238}U$ ages (650 ± 5 Ma) than the other 9 analyses, perhaps representing inheritance from the older rocks in the area. Spot SHI-1.3 has high common ^{206}Pb (1.06%) with a younger $^{206}Pb/^{238}U$ age than the other ten analyses (Table 2). Two other spots (SHI-1.4 and SHI-1.9) record slightly younger $^{206}Pb/^{238}U$ ages of 565 ± 5 (SHI-1.4) and 577 ± 5 Ma (SHI-1.9), which we interpret as due to a late thermal event, perhaps related to intrusion of post-tectonic granites or dikes. The remaining six analyses group tightly and define a concordia age of 629 ± 5 Ma (95% conf.; MSWD = 0.007; Fig. 7b), which we interpret as the age of crystallization.

4.5. Wadi Um Ashirah quartz-diorite

Sample ASH-1 (22.863°N, 33.217°E) is a quartz diorite collected from Wadi Um Ashirah (Fig. 3c) at the entrance of Wadi Allaqi near Lake Nasser. Field relationships indicate that it intruded the ophiolite nappe. Sample ASH-1 is medium to coarse-grained and hypidiomorphic (Fig. 4e). It consists of euhedral to subhedral altered plagioclase with margins embayed by quartz, well-formed prisms of hornblende partly altered to chlorite, anhedral quartz, biotite flakes partially altered to chlorite, and accessory zircon, apatite and Fe-oxides (Fig. 4e, f). Major element data (Table 1) show that sample ASH-1 has high SiO_2 (70%), moderate TiO_2 (0.61%), and low MgO (0.90%) and K_2O (0.55%). ASH-1 zircons are mostly euhedral, clear to yellow-brown, prismatic (~200 × 50 μm) and show well-developed oscillatory zoning consistent with a magmatic origin (Fig. 5e). One analysis was made on each of 12 zircons (Table 2) and these are presented on a concordia plot (Fig. 7c). With the exception of high U in spot ASH-1.8 (2722 ppm), zircon U contents are moderate (164–927 ppm) and Th/U ratios are low (0.18–0.44; Table 2). Spot ASH-1.8 also shows reverse discordance and records an older $^{206}Pb/^{238}U$ age (756 ± 6 Ma) than the other eleven analyses, perhaps reflecting xenocrysts derived from older material. The remaining 11 analyses cluster tightly, defining a concordia age of 709 ± 4 Ma (2σ; MSWD = 0.9; Fig. 7c), which is interpreted as the crystallization age of the quartz diorite.

5. Discussion

We now combine our new ages with published ages for the YOSHGAH suture in order to constrain the geologic evolution of the suture zone, especially the age of the ophiolites and when they were

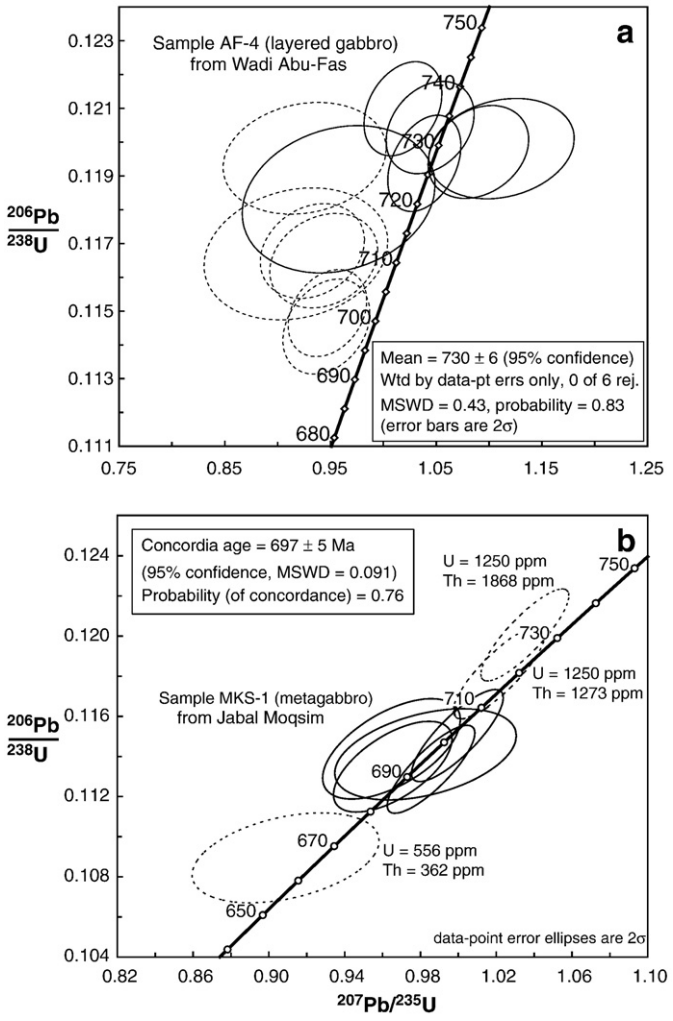

Fig. 6. U–Pb concordia diagrams of SHRIMP II data for zircons studied here (a) layered gabbro (sample AF-4) from Wadi Abu-Fas, and (b) gabbro (sample MKS-1) from Jabal Moqsim. Dashed ellipses indicate zircon analyses that were excluded from age calculations. Analytical data are given in Table 2.

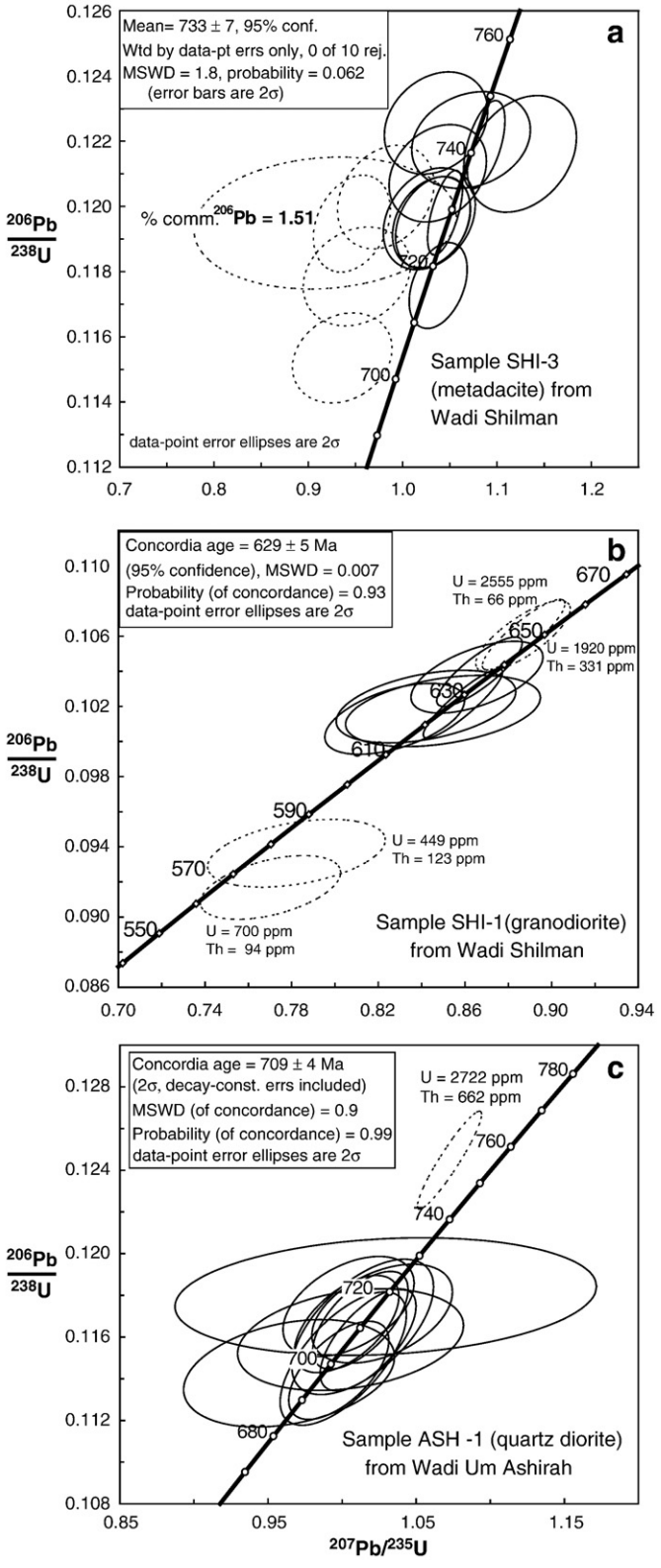

Fig. 7. U–Pb concordia diagrams of SHRIMP II data for zircons studied here: (a) metadacite (sample SHI-3) from Wadi Shilman, (b) granodiorite (sample SHI-1) from Wadi Shilman, and (c) quartz diorite (sample ASH-1) from Wadi Um Ashirah. Dashed ellipses indicate zircon analyses that were excluded from age calculations. Analytical data are given in Table 2.

emplaced. These ophiolites display a broad variability in lithology, geochemistry and chronology which rules out the simplest plate tectonic scenario (Martinez et al., 2009). Our results indicate that parts of the Allaqi ophiolite formed at ~730 Ma. This age is constrained by ophiolitic gabbro AF-4 (730 ± 6 Ma; Fig. 6a) and overlying metavolcanic rocks SHI-3 (733 ± 7 Ma; Fig. 7a). This age is indistinguishable from zircon ages from other Eastern Desert ophiolites, including Fawakhir (736.5 ± 1.5 Ma; Andresen et al., 2009), Ghadir (746 ± 19 Ma, Kröner et al., 1992) and Gerf (741 ± 21 Ma; Kröner et al., 1992). Sm–Nd dating also supports an age of ~750 Ma for the Gerf ophiolite (Zimmer et al., 1995). Nevertheless, the inference that the Allaqi–Gerf ophiolite formed at ~730–750 Ma conflicts with two other ages reported by Kröner et al. (1992): 770 ± 9 Ma for the dike at the mouth of Wadi Allaqi and 808 ± 14 Ma for the Onib plagiogranite.

A similar situation is seen for the YOSHGAH ophiolites across the Red Sea in Saudi Arabia. Two multigrain zircon aliquots from the Jabal al Wask ophiolitic gabbro gave two strongly discordant model upper concordia intercept ages of 751 ± 11 Ma and 772 ± 16 Ma (Pallister et al., 1988). Two multigrain samples from the Jabal al Wask plagiogranite yielded discordant model ages of 740 ± 11 Ma (Fig. 1, Pallister et al., 1988). In contrast, a single multigrain (discordant) fraction from the Jabal Ess ophiolitic gabbro gave a model upper intercept age of 780 ± 11 Ma (Pallister et al., 1988), identical to a Sm/Nd mineral isochron age of 782 ± 36 obtained for the same sample by Claesson et al. (1984).

It is unclear how to best explain the evidence that some YOSHGAH ophiolites formed at ~770–810 Ma and others formed at ~730–740 Ma. Such age variations are found all along the suture. At least three possible explanations can be explored: 1) The older ages reflect zircon xenocrysts. This explanation is plausible for the felsic dike at the entrance of Wadi Allaqi but less so for the Onib plagiogranite where all four grains yielded indistinguishable ages and cannot explain the Ess Sm/Nd age. Recognition that pre-Neoproterozoic zircons are common in ANS juvenile crust is increasingly reported (Hargrove et al., 2006a,b). Ali et al. (2009) reported also that 28 of 77 (36%) zircons analyzed from Central Eastern Desert of Egypt metavolcanic rocks have ages >900 Ma. They suggested that the interaction of mafic magmas with far-travelled glacigenic sediments was responsible for the pre-Neoproterozoic zircons; 2) YOSHGAH ophiolites could have formed at more than one time, for example as separate components of a complex arc–back arc basin system. Given that these are SSZ ophiolites, the older ages might reflect forearc crust that formed when subduction began, and the younger ages could reflect subsequent back-arc basin spreading (Stern et al., 2004); and 3) The Onib ophiolite defines a separate suture that should not be included as part of the YOSHGAH suture. Even if this is true, it does not explain the older ages obtained from the Allaqi felsic dike and the Jabal Ess ophiolite. At present, we prefer the second explanation, which suggests that ophiolites along the YOSHGAH suture formed at more than one time (Stern et al., 2004). Certainly the association of ophiolites with arc metavolcanic–volcaniclastic rocks and intruded by arc plutons, suggest that the ophiolite might have been arc basement (Dilek and Ahmed, 2003; Dilek et al., 2008). Further work is required to understand the significance of the variation in the formation ages of YOSHGAH ophiolites.

A second question that the new ages allow us to address when was the YOSHGAH ophiolite assemblage emplaced? For the Allaqi segment, the ophiolite appears to have been emplaced very soon after formation. This is constrained by our ages for cross-cutting plutons: (ASH-1; 709 ± 4 Ma and MKS-1; 697 ± 5 Ma) as well as by plutons dated by others (729 ± 17 Ma and 736 ± 11 Ma ages for Abu Swayel gabbro-diorite; Kröner et al., 1992). We note that the age reported for the Abu Swayel gabbro-diorite is indistinguishable from our age for the ophiolite and associated metavolcanic rocks and wonder if this body is not part of the ophiolite. Such speculation is encouraged by the fact that the Abu Swayel gabbro-diorite complex is intimately associated with ophiolitic serpentinites (similar to the situation for gabbro AF-4 730 ± 6 Ma) and is MORB-like in composition (Kröner et al., 1992). We also note that the ~700 Ma ages found for two of the five igneous rocks we dated are consistent with the 690–720 Ma episode of crust formation noted for NE Sudan and SE Egypt by Stern and Kröner (1993).

Based on our U–Pb zircon data, combined with published geochronology, geochemical and Nd isotope data, we propose a simplified evolutionary diagram (Fig. 8) to summarize the tectonic events in the northernmost ANS during Neoproterozoic time.

6. Conclusions

The layered gabbro associated with the serpentinite and talc-carbonates in Wadi Allaqi has an age of 730 ± 6 Ma, similar to the ophiolites in the Eastern Desert of Egypt at Fawakhir and Wadi Ghadir (736.5 ± 1.5 and 741 ± 21 Ma, respectively). The coeval generation of Eastern Desert ophiolites confirms the importance of the ~750 Ma crust-forming event in this region (Ali et al., 2009). Zircon ages of cross-cutting quartz diorite and the metagabbro plutons are ~700 Ma, confirming the importance of the 690–720 Ma crust forming event in NE Sudan and SE Egypt, and syn-tectonic granodiorite is 629 ± 5 Ma. Our analyses of Wadi Allaqi samples revealed no evidence of pre-Neoproterozoic zircons, further indicating that ANS crust in this region is mostly juvenile. Our most important conclusion is that the U–Pb zircon ages obtained from this study, combined with published zircon ages for the YOSHGAH suture, indicate that these ophiolites formed at more than one time. Oceanic crust represented by the ophiolite assemblage began to form as early as ~810 Ma, but all ages along the

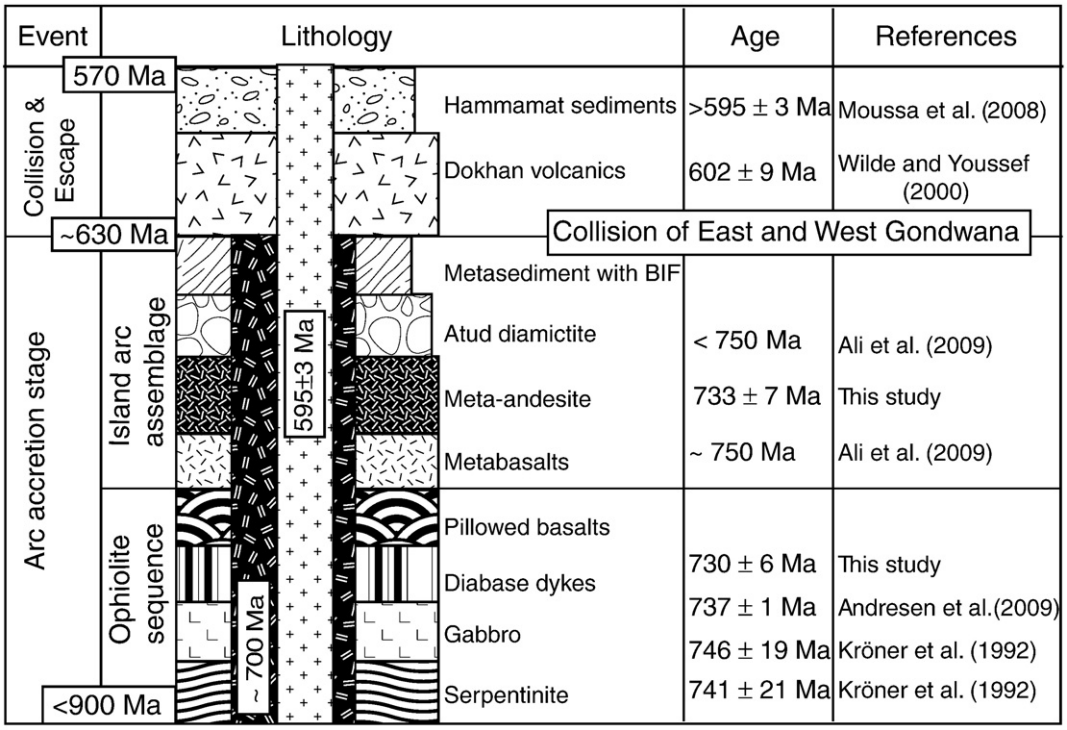

Fig. 8. Simplified evolutionary diagram shows major tectonic events of the Neoproterozoic basement complex in Egypt (modified from Stern, 1981; Moghazi, 2003). Ages from this study, Kröner et al. (1992), Ali et al. (2009), Moussa et al. (2008), Wilde and Youssef (2000).

westernmost Allaqi–Heiani segment formed considerably later at ~730–740 Ma. This ophiolite was obducted soon after it formed, indicating that collision between the South Eastern Desert–Midyan and Gabgaba–Gebeit–Hijaz terranes occurred at ~700 Ma.

Acknowledgments

This work was supported by NSF grant EAR-0804749 to RJS in collaboration with the National Research Centre (NRC) of Egypt and a post-doctoral fellowship from Curtin University of Technology in Perth, Australia to KAA. The SHRIMP II facility in Perth is operated jointly by Curtin University of Technology, the University of Western Australia and the Geological Survey of Western Australia, with support from the Australian Research Council. Constructive reviews of this manuscript by Prof. Alfred Kröner, Prof. Yildirim Dilek and an anonymous reviewer are gratefully acknowledged. We thank Editor-in-Chief Prof. M. Santosh for insightful comments and criticism that improved this manuscript. This is UTD Geosciences contribution number #1205 and TIGeR publication # 206.

References

Abd El-Naby, H.H., Frisch, W., 2002. Origin of the Wadi Haimur–Abu Swayel gneiss belt, south Eastern Desert, Egypt: petrological and geochronological constraints. Precambrian Research 113, 307–322.

Abd El-Naby, H.H., Frisch, W., Hegner, E., 2000. Evolution of the Pan-African Wadi Haimur metamorphic sole, Eastern Desert, Egypt. Journal of Metamorphic Geology 18, 639–651.

Abd El-Rahman, Y., Polat, A., Dilek, Y., Fryer, B.J., El-Sharkawy, M., Sakran, S., 2009a. Geochemistry and tectonic evolution of the Neoproterozoic incipient arc–forearc crust in the Fawakhir area, Central Eastern Desert of Egypt. Precambrian Research 175, 116–134.

Abd El-Rahman, Y., Polat, A., Dilek, Y., Fryer, B.J., El-Sharkawy, M., Sakran, S., 2009b. Geochemistry and tectonic evolution of the Neoproterozoic Wadi Ghadir ophiolite, Eastern Desert, Egypt. Lithos 113, 158–178.

Abdelsalam, M.G., Stern, R.J., 1996. Sutures and shear zones in the Arabian–Nubian Shield. Journal of African Earth Sciences 23, 289–310.

Abdelsalam, M.G., Abdeen, M.M., Dowaidar, H.M., Stern, R.J., Abdelghaffar, A.A., 2003. Structural evolution of the Neoproterozoic Western Allaqi–Heiani suture, south-eastern Egypt. Precambrian Research 124, 87–104.

Abdelsalam, M.G., Tsige, L., Yihunie, T., Hussien, B., 2008. Terrane rotation during the East African Orogeny: evidence from the Bulbul Shear Zone, south Ethiopia. Gondwana Research 14, 497–508.

Agar, R.A., Stacey, J.S., Whitehouse, M.J., 1992. Evolution of the southern Afif terrane — a geochronologic study. Saudi Arabian Deputy Ministry for Mineral Resource Open File Report DGMR-OF-10-15. 41 pp.

Ali, K.A., Stern, R.J., Manton, W.I., Kimura, J.-I., Khamees, H.A., 2009. Geochemistry, Nd isotopes and U–Pb SHRIMP zircon dating of Neoproterozoic volcanic rocks from the Central Eastern Desert of Egypt: new insights into the 750 Ma crust-forming event. Precambrian Research 171, 1–22.

Andresen, A., Abu El-Rus, M.A., Myhre, P.I., Boghdady, G.Y., Corfu, F., 2009. U–Pb TIMS age constraints on the evolution of the Neoproterozoic Meatiq Gneiss Dome, Eastern Desert, Egypt. International Journal of Earth Sciences 98, 481–497.

Azer, M.K., Stern, R.J., 2007. Neoproterozoic (835–720 Ma) serpentinites in the Eastern Desert, Egypt: fragments of forearc mantle. Geology 115, 457–472.

Bakor, A.R., Gass, I.G., Neary, C.R., 1976. Jabal al Wask, northwest Saudi Arabia: an Eocambrian back-arc ophiolite. Earth and Planetary Science Letters 30, 1–9.

Berhe, S.M., 1990. Ophiolites in Northeast and East Africa: implications for Proterozoic crustal growth. Journal of the Geological Society of London 147, 41–57.

Claesson, S., Pallister, J.S., Tatsumoto, M., 1984. Samarium–neodymium data on two late Proterozoic ophiolites of Saudi Arabia and implications for crustal and mantle evolution. Contributions to Mineralogy and Petrology 85, 244–252.

Dilek, Y., Ahmed, Z., 2003. Proterozoic ophiolites of the Arabian Shield and their significance in Precambrian tectonics. Ophiolites in Earth History: Journal of the Geological Society of London, Special Publications, 218, pp. 685–701.

Dilek, Y., Furnes, H., Shallo, M., 2007. Suprasubduction zone ophiolite formation along the periphery of Mesozoic Gondwana. Gondwana Research 11, 453–475.

Dilek, Y., Furnes, H., Shallo, M., 2008. Geochemistry of the Jurassic Mirdita ophiolites (Albania) and the MORB to SSZ evolution of a marginal basin oceanic crust. Lithos 100, 174–209.

El Gaby, S., List, F.K., Tehrani, R., 1988. Geology, evolution and metallogenesis of the Pan-African Belt in Egypt. In: El Gaby, S., Greiling, R.O. (Eds.), The Pan African Belt of Northeast Africa and adjacent areas. Vieweg & Sohn, Braunschweig/Wiesbaden, pp. 17–68.

El-Bialy, M.Z., 2010. On the Pan-African transition of the Arabian–Nubian Shield from compression to extension: the post-collision Dokhan volcanic suite of Kid-Malhak region, Sinai, Egypt. Gondwana Research 17, 26–43.

El-Kazzaz, Y.A., Taylor, W.E.G., 2001. Tectonic evolution of the Allaqi Shear zone and implications for Pan-African terrane amalgamation in the southern Eastern Desert, Egypt. Journal of African Earth Sciences 33, 177–197.

El-Nisr, S., 1997. Late Precambrian volcanism at Wadi Allaqi, south Eastern Desert, Egypt: evidence for transitional continental arc/margin environment. Journal African Earth Sciences 24, 301–313.

Frisch, W., Al-Shanti, A.M., 1977. Ophiolite belts and the collision of island arcs in the Arabian Shield. Tectonophysics 43, 293–306.

Gahlan, H.A., Arai, S., 2009. Carbonate–orthopyroxenite lenses from the Neoproterozoic Gerf ophiolite, South Eastern Desert, Egypt: the first record in the Arabian Nubian Shield ophiolites. Journal of African Earth Sciences 53, 70–82.

Hargrove, U.S., Stern, R.J., Kimura, J.I., Manton, W.I., Johnson, P.R., 2006a. How juvenile is the Arabian–Nubian Shield? Evidence from Nd isotopes and pre-Neoproterozoic inherited zircon in the Bi'r Umq suture zone, Saudi Arabia. Earth and Planetary Science Letters 252, 308–326.

Hargrove, U.S., Stern, R.J., Griffin, W.R., Johnson, P.R., Abdelsalam, M.G., 2006b. From island arc to craton: timescales of crustal formation along the Neoproterozoic Bi'r Umq Suture zone, Kingdom of Saudi Arabia. Saudi Geological Survey Technical Report SGS-TR-2006-6. 69 pp.

Jacobs, J., Thomas, R.J., 2004. Himalayan-type indenter-escape tectonics model for the southern part of the late Neoproterozoic–early Paleozoic East African-Antarctic orogen. Geology 32, 721–724.

Johnson, P.R., Woldehaimanot, B., 2003. Development of the Arabian–Nubian Shield: perspectives on accretion and deformation in the northern East African Orogen and the assembly of Gondwana. In: Yoshida, M., Dasgupta, S., Windley, B. (Eds.), Proterozoic East Gondwana: Supercontinent Assembly and Breakup: Geological Society of London Special Publications, 206, pp. 289–325.

Kröner, A., 1985. Ophiolites and the evolution of tectonic boundaries in the late Proterozoic Arabian–Nubian Shield of northeast Africa and Arabia. Precambrian Research 27, 277–300.

Kröner, A., Linnebacher, P., Stern, R.J., Reischmann, T., Manton, W.I., Hussein, I.M., 1991. Evolution of Pan-African island arc assemblages in the southern Red Sea Hills, Sudan and in southwestern Arabia as exemplified by geochemistry and geochronology. Precambrian Research 53, 99–118.

Kröner, A., Todt, W., Hussein, I.M., Mansour, M., Rashwan, A.A., 1992. Dating of late Proterozoic ophiolites in Egypt and the Sudan using the single grain zircon evaporation technique. Precambrian Research 59, 15–32.

Kusky, T.M., Ramadan, T.M., 2002. Structural controls on Neoproterozoic mineralization in the South Eastern Desert, Egypt: an integrated field, Landsat TM, and SIR-C/X SAR approach. Journal of African Earth Sciences 35, 107–121.

Küster, D., Liégeois, J.P., Matukov, D., Sergeev, S., Lucassen, F., 2008. Zircon geochronology and Sr, Nd, Pb isotope geochemistry of granitoids from Bayuda Desert and Sabaloka (Sudan): evidence for a Bayudian event (920–900 Ma) preceding the Pan-African orogenic cycle (860–590 Ma) at the eastern boundary of the Saharan Metacraton. Precambrian Research 164, 16–39.

Martinez, S.S., Arenas, R., Femández-Suárez, J., Jeffries, T., 2009. From Rodinia to Pangaea: ophiolites from NW Iberia as witness for a long-lived continental margin. Journal of the Geological Society of London, Special Publications 327, 317–341.

Moghazi, A.M., 2003. Geochemistry and petrogenesis of a high-K calc-alkaline Dokhan Volcanic suite, South Safaga area, Egypt: the role of late Neoproterozoic crustal extension. Precambrian Research 125, 161–178.

Moussa, E.M.M., Stern, R.J., Manton, W.I., Ali, K.A., 2008. SHRIMP zircon dating and Sm/Nd isotopic investigations of Neoproterozoic granitoids, Eastern Desert, Egypt. Precambrian Research 160, 341–356.

Nassief, M.O., Macdonald, R., Gass, I.G., 1984. The Jebel Thurwah Upper Proterozoic Ophiolite Complex, western Saudi Arabia. Journal of the Geological Society of London 141, 537–546.

Nelson, D.R., 1997. Complication of SHRIMP U–Pb zircon geochronology data. 1996: Geological Survey of Western Australia, Record 1997/2. 189 pp.

Pallister, J.S., Stacey, J.S., Fischer, L.B., Premo, W.R., 1988. Precambrian ophiolites of Arabia; geologic setting, U–Pb geochronology, Pb-isotope characteristics, and implications for continental accretion. Precambrian Research 38, 1–54.

Pearce, J.A., Robinson, P.T., 2010. The Troodos ophiolitic complex probably formed in a subduction initiation, slab edge setting. Gondwana Research 18, 60–81.

Pidgeon, R.T., Furfaro, D., Kennedy, A.K., Nemchin, A.A., Van Bronswijk, W., 1994. Calibration of zircon standards for the Curtin SHRIMP II. Eight International Conference on Geochronology, Cosmochronology and Isotope Geology: U.S. Geological Survey Circular, 1107, p. 251. Berkeley, USA. Abstract Vol.

Shanti, M., Roobol, M.J., 1979. A late Proterozoic ophiolite complex at Jabal Ess in northern Saudi Arabia. Nature 279, 488–491.

Stern, R.J., 1981. Petrogenesis and tectonic setting of Late Precambrian ensimatic volcanic rocks, Central Eastern Desert of Egypt. Precambrian Research 16, 195–230.

Stern, R.J., 1994. Arc assembly and continental collision in the Neoproterozoic East African Orogen: implications for the consolidation of Gondwanaland. Annual Reviews of Earth and Planetary Science 22, 319–351.

Stern, R.J., 2008. Neoproterozoic crustal growth: the solid Earth system during a critical episode of Earth history. Gondwana Research 14, 33–50.

Stern, R.J., Kröner, A., 1993. Geochronologic and isotopic constraints on late Precambrian crustal evolution in NE Sudan. Geology 101, 555–574.

Stern, R.J., Kröner, A., Manton, W.I., Reischmann, T., Mansour, M., Hussein, I.M., 1989. Geochronology of late Precambrian Hamisana shear zone, Red Sea Hills, Sudan and Egypt. Journal of the Geological Society of London 146, 1017–1029.

Stern, R.J., Nielsen, K.C., Best, E., Sultan, M., Arvidson, R.E., Kröner, A., 1990. Orientation of late Precambrian sutures in the Arabian–Nubian Shield. Geology 18, 1103–1106.

Stern, R.J., Kröner, A., Bender, R., Reischmann, T., Dawoud, A.S., 1994. Precambrian basement around Wadi Halfa, Sudan: a new perspective on the evolution of the East Saharan Craton. Geologische Rundschau 83, 564–577.
Stern, R.J., Johnson, P.J., Kröner, A., Yibas, B., 2004. Neoproterozoic ophiolites of the Arabian–Nubian Shield. In: Kusky, T. (Ed.), Precambrian Ophiolites. Elsevier, pp. 95–128.
Stoeser, D.B., Camp, V.E., 1985. Pan-African microplate accretion of the Arabian Shield. Geological Society of America Bulletin 96, 817–826.
Whitehouse, M.J., Stoeser, D., Stacey, J.S., 2001. The Khida Terrane — geochronological and Isotopic Evidence for Paleoproterozoic and Archean Crust in the Eastern Arabian Shield of Saudi Arabia. Gondwana Research 4, 200–202.
Wilde, S.A., Youssef, K., 2000. Significance of SHRIMP U–Pb dating of Imperial Porphyry and associated Dokhan Volcanics, Gebel Dokhan, north Eastern Desert, Egypt. Journal of African Earth Sciences 31, 403–413.
Williams, I.S., 1998. U–Th–Pb geochronology by ion microprobe. Reviews in Economic Geology 7, 1–35.
Zimmer, M., Kröner, A., Jochum, K.P., Reischmann, T., Todt, W., 1995. The Gabal Gerf complex: a Precambrian N-MORB ophiolite in the Nubian Shield, NE Africa. Chemical Geology 123, 29–51.
Zoheir, B.A., Klemm, D.D., 2007. The tectono-metamorphic evolution of the central part of the Neoproterozoic Allaqi–Heiani suture, south Eastern Desert of Egypt. Gondwana Research 12, 289–304.